Proceeding of the IEEE
International Conference on Robotics and Biomimetics
Dali, China, December 2019

Sensorless Hybrid Normal-Force Controller With Surface Prediction

Yingjie Qian
School of Mechanical Engineering
Shanghai Jiaotong University
Shanghai, China
qyjyork@sjtu.edu.cn

Jianjun Yuan, Sheng Bao
Shanghai Robotics Institute
Shanghai University
Shanghai, China
terabit@shu.edu.cn

Liming Gao
Mechanical Engineering
Penn State University
Pennsylvania, USA
winstonglm@gmail.com

***Abstract* - In this paper, an improved sensorless hybrid controller for constant force control along normal direction is proposed for applications including polishing, milling and deburring. No additional sensors are involved. External joint torques of all joints can be calculated from their electric current, dynamic model and friction model. With the help of dynamically consistent generalized inverse matrix, they can be converted to external force/torque at the end-effector. The underlying force control strategy is the integration of impedance control model and explicit force control. The novel improvement is the real-time prediction algorithm of surface's shape profile and normal direction without any prior knowledge. So, this force controller has great adaptiveness to arbitrary unknown surfaces. Experiments were performed on a 7 degrees-of-freedom (DOFs) robot to test the controller's capability and utility on an inclined plane and curved surface. Results prove the credibility of external force estimation. The normal force tracking accuracy is adequate for targeted applications. Real-time prediction is functional as the robot adjusts its orientation accordingly.**

Index Terms – Sensorless Force Control, Hybrid Force Control, Shape Profile Prediction, Normal Direction Prediction

I. INTRODUCTION

Deburring, milling and polishing are important manufacture methods for surface improvement. The amount of material to be removed is directly related with the contact force exerted on surface [1, 2]. However, manual operation generally cannot meet the requirement of contact force, thus may adversely impact the machining quality. Moreover, the working condition of these methods is hazardous for human workers due to mass vibration, loud noise and heavy dust. So collaborative robot arms have become the ideal replacement of workers in these applications [3, 4].

Force control schemes are used to achieve the requirement of contact force at robot's end-effector [5]. The contact force is, in general, measured by a force sensor mounted at end-effector, or joint torque sensors in individual joints. Yet, those sensors may cause substantial cost increase, and the hostile working condition makes them vulnerable. So, sensorless force control is of great academic and practical importance [6-8].

Gao et. al proposed a thorough study on the joint torque estimation based on electric current information and joint friction model, and applied it on a single joint [8]. Building on his work, in this paper, external torques of all robot joints are calculated and converted to the external force/torque at end-effector by using force Jacobian matrix. Since the robot used in this paper has 7DOFs (as is depicted in Fig. 1), dynamically consistent generalized inverse matrix is applied [9]. Singularity issues are not discussed due to space limitations.

Different control schemes have been proposed to achieve active force control. Ott et al. designed an impedance force controller for flexible joint robots based on passivity [10]. Roveda et al. studied the situation where the dynamic parameters of the environment are uncertain building on the impedance-based force control [11]. Other force control schemes include sliding model control [1, 12], admittance control with artificial skin [13] and additional smart end-effector tool [3, 14].

Building on impedance control, hybrid control methods have attracted more attention. Schindlbeck et al. proposed a hybrid force controller with the help of task-energy tanks for better stability [15]. Shahriari et al. applied the concept of learning by demonstration into the passivity-based force tracking to achieve adaptive performance to planes with different slopes [16]. The adopted hybrid force control scheme in this work is based on the impedance control model combined with explicit force control under the consideration of robustness, accuracy and convenience. Yuan et. al studied surface tracking with constant force along the gravitational direction [17].

Yet, few researches focus on force control along the normal direction of the surface. As a matter of fact, force tracking along normal direction would be more reasonable and effective for machining, especially when the robot can change its orientation accordingly.

In this paper, an improved sensorless hybrid normal-force controller is proposed to maintain constant normal contact force. The novel improvement is the prediction algorithms including the shape profile and normal direction prediction of arbitrary unknown surfaces which improves control accuracy and utility. Additionally, the robot will also adjust its end-effector's orientation to the normal direction.

This paper is organized as follows with six sections. Section II discusses the estimation of external force/torque at end-effector. A hybrid position-based force controller integrating impedance control and explicit force control is introduced in Section III. In Section IV, prediction algorithms of surface shape profile and normal direction are explained and followed by verification experiments on a 7-DOF collaborative robot in Section V. Experiments include tracking along an inclined plane and a curved surface. Finally, Section VI makes the conclusion.

978-1-7281-6321-5/19//$31.00 ©2019 IEEE

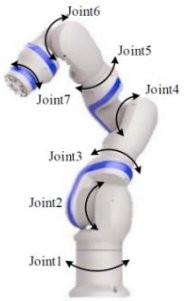

Fig. 1 The 7DOF collaborative robot used in this work.

II. External Force\Torque Estimation

A. Calculation of External Joint Torque

The dynamic model of a flexible joint with velocity-load friction model can be written as follows [8].

$$\boldsymbol{\tau_s} = \boldsymbol{\tau_d} + \boldsymbol{\tau_f} - \boldsymbol{\tau_{ext}} \tag{1}$$

$$\boldsymbol{\tau_s} = \boldsymbol{N}(\boldsymbol{K_t}\boldsymbol{I} - \boldsymbol{J_m}\ddot{\boldsymbol{\theta}}) \tag{2}$$

$$\boldsymbol{\tau_d} = \boldsymbol{M}(\boldsymbol{q})\ddot{\boldsymbol{q}} + \boldsymbol{C}(\boldsymbol{q},\dot{\boldsymbol{q}})\dot{\boldsymbol{q}} + \boldsymbol{G}(\boldsymbol{q}) \tag{3}$$

$$\begin{aligned}\tau_f(\dot{q},\tau_l) = &\left[\alpha_c + \left(\alpha_{cl} + \alpha_{sl}e^{-|\dot{q}/\beta_l|}\right)|\tau_l|\right]\mathrm{sgn}(\dot{q}) \\ &+\alpha_v\left(1 - e^{-|\dot{q}/\beta_v|}\right)\mathrm{sgn}(\dot{q})\end{aligned} \tag{4}$$

Herein, $\boldsymbol{\tau_s}$ stands for the output torque vector of motors after the speed reducer, $\boldsymbol{\tau_d}$ for the dynamic torque vector, $\boldsymbol{\tau_f}$ for the joint friction vector and $\boldsymbol{\tau_{ext}}$ for the external joint torque vector.

$\boldsymbol{K_t}$, $\boldsymbol{J_m}$ and $\boldsymbol{N}$ are diagonal matrices of joints' torque-current coefficients, equivalent rotation inertia and speed reduction ratios respectively. $\boldsymbol{I}$ is the vector of electric current and $\boldsymbol{\theta}$ is vector of motor angles.

$\boldsymbol{q}$ is the vector of joint angles. $\boldsymbol{M}(\boldsymbol{q})$ denotes the inertia matrix, $\boldsymbol{C}(\boldsymbol{q},\dot{\boldsymbol{q}})$ the Coriolis and centrifugal matrix and $\boldsymbol{G}(\boldsymbol{q})$ the gravitational torque vector. The friction torque is analysed in scalar form. α_c is the constant static friction. α_v, β_l and β_v are velocity-related friction parameters. α_{cl} and α_{sl} are load-related friction parameters. τ_l is the load torque for an individual joint which is the same as the corresponding element from $\boldsymbol{G}(\boldsymbol{q})$. Due to space limitation, tuning of friction parameters will not be discussed in detail. Gao et. al provided a comprehensive method [8].

Once $\boldsymbol{\tau_s}$, $\boldsymbol{\tau_d}$ and $\boldsymbol{\tau_f}$ have been obtained, $\boldsymbol{\tau_{ext}}$ can be calculated accordingly. Note that a first-order signal filter is applied on $\ddot{\boldsymbol{q}}$ to reduce the noise. Since each robot joint is equipped with two encoders, one measuring the angle of motor and the other measuring the angle of link, there's no necessity to consider joint's intrinsic elasticity.

B. Conversion to External Force at End-effector

Relation between joint angles and posture of end-effector, and their derivatives are given by

$$\boldsymbol{X} = \boldsymbol{f}(\boldsymbol{q}) \tag{5}$$

$$\dot{\boldsymbol{X}} = \boldsymbol{J}\,\dot{\boldsymbol{q}} \tag{6}$$

$\boldsymbol{X}$ stands for the 6-dimensional posture vector of end-effector including position and orientation in Cartesian space. $\boldsymbol{f}()$ encodes the forward kinematic transformation function. $\boldsymbol{J}$ is called the Jacobian matrix, connecting the Cartesian space and joint space. It is a function of $\boldsymbol{q}$.

By applying the principle of virtual work, external joint torques and external force at end-effector are ruled by [5]

$$\boldsymbol{\tau_{ext}} = \boldsymbol{J}^T\,\boldsymbol{F_{ext}} \tag{7}$$

$$\boldsymbol{F_{ext}} = (\boldsymbol{J}^T)^{\dagger}\boldsymbol{\tau_{ext}} \tag{8}$$

Herein, $\boldsymbol{F_{ext}}$ denotes the 6-dimensional external force/torque vector at end-effector. $\boldsymbol{J}^T$ is the transpose of Jacobian matrix, which is also called the force Jacobian matrix.

The dynamically consistent generalized inverse matrix of Jacobian matrix, $(\boldsymbol{J}^T)^{\dagger}$, is used for robots with redundant DOF. In this case, Moore-Penrose generalized inverse matrix is applied. Singular cases are excluded. As a matter of fact, this sensorless estimation method for external force/torque at end-effector by using current information can also be promoted to industrial robots. In this paper, only the part of external force is concerned.

III. Hybrid Position-Based Force Controller

A. Dynamic Model in Cartesian Space

The robot dynamic model in joint space can be deduced from (1) to (8) as

$$\boldsymbol{\tau_s} = \boldsymbol{M}(\boldsymbol{q})\ddot{\boldsymbol{q}} + \boldsymbol{C}(\boldsymbol{q},\dot{\boldsymbol{q}})\dot{\boldsymbol{q}} + \boldsymbol{G}(\boldsymbol{q}) + \boldsymbol{\tau_f} - \boldsymbol{J}^T\boldsymbol{F_{ext}} \tag{9}$$

However, it would be more intuitive if the control strategy is applied in Cartesian space.

The second derivative of (6) is given by

$$\ddot{\boldsymbol{X}} = \boldsymbol{J}\,\ddot{\boldsymbol{q}} + \dot{\boldsymbol{J}}\,\dot{\boldsymbol{q}} \tag{10}$$

By multiplying $\boldsymbol{JM^{-1}(q)}$ to both sides of (9) and reorganizing, one can get the dynamic model of robot in Cartesian space.

$$\boldsymbol{M_x}\ddot{\boldsymbol{X}} + \boldsymbol{C_x}\dot{\boldsymbol{X}} + \boldsymbol{G_x} = (\boldsymbol{J}^T)^{\dagger}(\boldsymbol{\tau_s} - \boldsymbol{\tau_f}) + \boldsymbol{F_{ext}} \tag{11}$$

$$\boldsymbol{M_x} = (\boldsymbol{J}\boldsymbol{M}^{-1}(\boldsymbol{q})\boldsymbol{J}^T)^{-1} \tag{12}$$

$$\boldsymbol{C_x} = (\boldsymbol{J}^T)^{\dagger}\boldsymbol{C}(\boldsymbol{q},\dot{\boldsymbol{q}}) - \boldsymbol{M_x}\dot{\boldsymbol{J}}\dot{\boldsymbol{q}} \tag{13}$$

$$\boldsymbol{G_x} = (\boldsymbol{J}^T)^{\dagger}\boldsymbol{G}(\boldsymbol{q}) \tag{14}$$

As it should be, (9) and (11) are two descriptions of the same robot system in different space, sharing similar forms.

B. Impedance Model in Cartesian Space

The guiding principle of impedance control is to model the interaction between the manipulator and the environment as a mass-spring-damp system [10]. Generally speaking, control schemes that build on impedance control can be classified into two types, the position-based impedance control and the force-based impedance control [18]. For position-based impedance model, the deviation of external force is the input while the output is position amendment command. In this paper, the position-based impedance control is adopted due to its better dependability. A reference trajectory is necessary.

The impedance control model is described by

$$\boldsymbol{U} = \boldsymbol{F_{ext}} - \boldsymbol{F_d} = \boldsymbol{B_x}\ddot{\boldsymbol{e}} + \boldsymbol{D_x}\dot{\boldsymbol{e}} + \boldsymbol{K_x}\boldsymbol{e} \tag{15}$$

$$\boldsymbol{e} = \boldsymbol{x_d} - \boldsymbol{x_r} \tag{16}$$

Herein, $\boldsymbol{U}$ stands for the force deviation between actual external force, $\boldsymbol{F_{ext}}$, and desired contact force $\boldsymbol{F_d}$. The position amendment command is denoted by $\boldsymbol{e}$, with $\boldsymbol{x_r}$ being the original reference position, $\boldsymbol{x_d}$ being the new demand position. The orientation of end-effector is not discussed in this part. $\boldsymbol{B_x}$, $\boldsymbol{D_x}$ and $\boldsymbol{K_x}$ denote the inertia matrix, the damping matrix and the stiffness matrix of the impedance model respectively.

The application of impedance control can achieve a compliant behaviour of the manipulator, yet cannot guarantee the contact force to be constant due to the existence of steady-state error [19].

When the system reaches a steady state, $\dot{\boldsymbol{e}}$ and $\ddot{\boldsymbol{e}}$ will become zero. Assume that the external force is provided by an elastic environment with stiffness of $\boldsymbol{K_e}$ at position $\boldsymbol{x_e}$.

$$\boldsymbol{F_{ext}} - \boldsymbol{F_d} = \boldsymbol{K}_x(\boldsymbol{x_d} - \boldsymbol{x_r}) \tag{17}$$

$$\boldsymbol{F_{ext}} = \boldsymbol{K_e}(\boldsymbol{x_e} - \boldsymbol{x_d}) \tag{18}$$

So, the steady-state force error, $\Delta\boldsymbol{F}_{ss}$ can be written as

$$\begin{aligned}\Delta\boldsymbol{F_{ss}} &= \boldsymbol{F_{ext}} - \boldsymbol{F}_d \\ &= (\boldsymbol{K_x} + \boldsymbol{K_e})^{-1}\boldsymbol{K_x}[\boldsymbol{K_e}(\boldsymbol{x_e} - \boldsymbol{x_r}) - \boldsymbol{F_d}]\end{aligned} \tag{19}$$

There're two ways to eliminate steady-state error. One is the regulation of parameters which will be discussed in the next section. The other one is the usage of force deviation integral, which is the idea from explicit force control. The integral of force deviation at time T_0, denoted as $\boldsymbol{\omega}(T_0)$, is defined as

$$\boldsymbol{\omega}(T_0) = \eta\int_0^{T_0}[\boldsymbol{F_{ext}}(t) - \boldsymbol{F_d}(t)]\ dt \tag{20}$$

η is the proportional factor. Equation (15) can be thus modified into

$$\boldsymbol{U} + \eta\int_0^{T_0} U(t)\ dt = \boldsymbol{B_x}\ddot{\boldsymbol{e}} + \boldsymbol{D_x}\dot{\boldsymbol{e}} + \boldsymbol{K_x}\boldsymbol{e} \tag{21}$$

C. Hybrid Position-based Control

The block diagram of position-based hybrid control is demonstrated in Fig. 2.

Position amendment $\boldsymbol{e}$ given by (21) is in continuous time domain. However, in programming, it should be converted to discrete form. The difference expression of $\boldsymbol{e}$ in discrete time domain is

$$\begin{aligned}\boldsymbol{e}(j) = (&\boldsymbol{B_x}T^{-2} + \boldsymbol{D_x}T^{-1} + \boldsymbol{K_x})^{-1} * \\ &[(2\boldsymbol{B_x}T^{-2} + \boldsymbol{D_x}T^{-1})\boldsymbol{e}(j-1) \\ &-\boldsymbol{B_x}T^{-2}\boldsymbol{e}(j-2) + \boldsymbol{U}(j) + \boldsymbol{\omega}(j)]\end{aligned} \tag{22}$$

where

$$\boldsymbol{\omega}(j) = \boldsymbol{\omega}(j-1) + \eta T[\boldsymbol{F_{ext}}(j) - \boldsymbol{F_d}(j)] \tag{23}$$

j is the discrete index, and T is the control period. $\boldsymbol{e}(j)$ denotes the position amendment at discrete time $t = jT$. $\boldsymbol{e}(0)$ is usually set to be 0 for stability concerns. $\boldsymbol{U}(j)$ and $\boldsymbol{\omega}(j)$ have similar meanings.

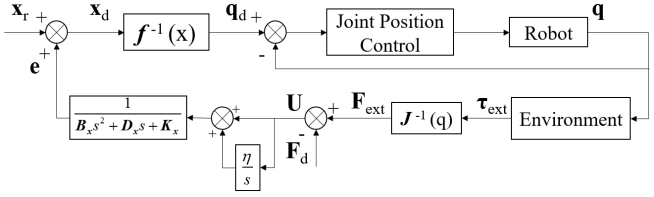

Fig. 2 Position-based hybrid control scheme in Cartesian Space.

So, the demand position $\boldsymbol{x_d}$ becomes

$$\boldsymbol{x_d}(j) = \boldsymbol{x_r}(j) + \boldsymbol{e}(j) \tag{24}$$

Since the position-based impedance model is applied, the demand position $\boldsymbol{x_d}$, including the original reference position and force-related amendment, should be converted to joint position $\boldsymbol{q_d}$ with the usage of inverse kinematics. The inner joint position control loop, provided by the robot platform itself, will execute this position amendment. It can be concluded that the force control is achieved through task space formulation while the final command is executed in joint space.

Practically speaking, not all dimensions require force control. In this paper, the constant force control is applied on the normal direction of the surface. Only the normal force component is effective. And $\boldsymbol{e}$ also follows that direction. Parameter matrices of the impedance model, $\boldsymbol{B_x}$, $\boldsymbol{D_x}$ and $\boldsymbol{K_x}$ can be simplified as scalars. The calculation of normal direction will be discussed in the next section.

IV. Improved Force Controller With Surface Prediction

A. Prediction of Surface's Shape Profile

As is analysed above, the regulation of parameters can also help eliminate the steady-state error. However, practical experiments show that the absence of stiffness $\boldsymbol{K_x}$ will cause instability. So only the reference trajectory, $\boldsymbol{x_r}$, can be regulated.

Obviously, if the reference trajectory is chosen to be

$$\boldsymbol{x_r} = \boldsymbol{x_e} - \boldsymbol{K_e}^{-1}\boldsymbol{F_d} \tag{25}$$

the error will become zero.

Noting that $\boldsymbol{K_e}^{-1}\boldsymbol{F_d}$ which is the deformation of the environment, is negligible since the environment is a metal surface, (24) can be simplified as

$$\boldsymbol{x_r} = \boldsymbol{x_e} \tag{26}$$

Apparently, this problem turns into the acquisition of the shape profile of an arbitrary surface, which will serve as the reference trajectory.

Prior acquisition of surface's shape profile usually causes an increase of hardware cost and time consumption [20]. So real-time prediction based on a pre-set trajectory is more feasible and universal.

In this paper, the pre-set reference trajectory, denoted as $\boldsymbol{x_{r0}}$, is considered to be horizontal in initial. While the robot moves along the trajectory, it predicts the vertical position of the surface in real-time, and adjusts accordingly. Since the deformation of surface is negligible, historical information of end-effector's position can be used to predict the shape profile.

$\boldsymbol{x_{r0}}$ can be decomposed into $x_{r0}(j)$, $y_{r0}(j)$ and $z_{r0}(j)$, denoting the x-axis, y-axis and z-axis components at time $t = jT$. x_i, y_i and z_i are the positions of end-effector relative to world coordinate in the past 100 control periods with i from 1 to 100. $\bar{x}$, $\bar{y}$ and $\bar{z}$ stand for corresponding average values.

The predicted reference trajectory, $\boldsymbol{x_r}$. has the same x-axis and y-axis components as $\boldsymbol{x_{r0}}$. Only its z-axis component, $z_r(j)$ needs adjustment.

$$z_r(j) = z_r(j-1) + \Delta z_r(j) \tag{27}$$

$z_r(0)$ is the initial z-axis value of the horizontal pre-set trajectory. $\Delta z_r(j)$ is the adjustment according to surface prediction, given by

$$\begin{aligned}\Delta z_r(j) = a_x[x_{r0}(j) - x_{r0}(j-1)] \\ + a_y[y_{r0}(j) - y_{r0}(j-1)]\end{aligned} \tag{28}$$

a_x and a_y are factors that can be obtained from the historical position information by using linear regression.

$$a_x = \left(L_{10}L_{22} - L_{20}L_{21}\right) / \left(L_{11}L_{22} - L_{12}L_{21}\right) \tag{29}$$

$$a_y = \left(L_{20}L_{22} - L_{10}L_{21}\right) / \left(L_{11}L_{22} - L_{12}L_{21}\right) \tag{30}$$

with

$$\begin{aligned}L_{10} &= \sum_{i=1}^{100}(x_i - \bar{x})(z_i - \bar{z}), L_{11} = \sum_{i=1}^{100}(x_i - \bar{x})^2 \\ L_{20} &= \sum_{i=1}^{100}(y_i - \bar{y})(z_i - \bar{z}), L_{22} = \sum_{i=1}^{100}(y_i - \bar{y})^2 \\ L_{12} &= \sum_{i=1}^{100}(x_i - \bar{x})(y_i - \bar{y})\end{aligned} \tag{31}$$

Combining with the position amendment, the demand position can be written as

$$\begin{aligned}\boldsymbol{x_d}(j) &= \boldsymbol{x_r}(j) + \boldsymbol{e}(j) \\ &= \boldsymbol{x_{r0}}(j) + \Delta\boldsymbol{x_r}(j) + \boldsymbol{e}(j)\end{aligned} \tag{32}$$

with

$$\Delta\boldsymbol{x_r}(j) = \left(\boldsymbol{0}_{1x2} \quad z_r(j) - z_r(0)\right)^T \tag{33}$$

It's worth mentioning that the prior knowledge of surface's shape profile will still undoubtedly improve the control performance. Yet In this paper, the control strategy without prior information is finally adopted to fully test its universality and capability.

B. Prediction of Surface's Normal Direction

The surface normal direction is necessary for force decomposition and robot's orientation adjustment. Here in this part, orientation amendment, which is parallel to position amendment, will be discussed.

Fig. 3 demonstrates the tracking process and force analysis. Prediction of normal direction cannot be obtained merely from historical position information. Historical force information is also involved.

The direction of friction can be considered opposite to the moving direction of end-effector.

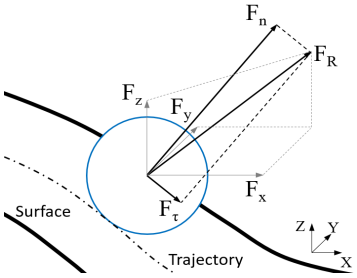

Fig. 3 Force analysis in the tracking process.

$$\boldsymbol{s_f} = \Delta\boldsymbol{x_r}(j) / \left|\Delta\boldsymbol{x_r}(j)\right| \tag{34}$$

$\boldsymbol{s_f}$ is the moving direction of end-effector after normalization

So $\boldsymbol{F_\tau}$ can be deduced as the component of $\boldsymbol{F_R}$ along $\boldsymbol{s_f}$.

$$\boldsymbol{F_\tau} = \boldsymbol{F_R} \bullet (-\boldsymbol{s_f}) \tag{35}$$

Finally, the normal force $\boldsymbol{F_n}$ is considered to be the residual component of $\boldsymbol{F_R}$ after the deduction of $\boldsymbol{F_\tau}$

$$\boldsymbol{F_n} = \boldsymbol{F_R} + \boldsymbol{F_R} \bullet \boldsymbol{s_f} \tag{36}$$

The normal direction, $\boldsymbol{s_n}$, is thus given by

$$\boldsymbol{s_n} = \boldsymbol{F_n} / \left|\boldsymbol{F_n}\right| \tag{37}$$

The robot can adjust the end-effector's orientation with a simple proportional controller by comparing its present z-axis of end-effector coordinate with $\boldsymbol{s_n}$.

Denote the orientation matrix of end-effector as $\boldsymbol{R_i}$.

$$\boldsymbol{R_i} = \left(\boldsymbol{R_{ix}} \quad \boldsymbol{R_{iy}} \quad \boldsymbol{R_{iz}}\right) \tag{38}$$

Here, $\boldsymbol{R_{ix}}$, $\boldsymbol{R_{iy}}$ and $\boldsymbol{R_{iz}}$ are three columns of $\boldsymbol{R_i}$, representing the x-, y- and z-axis of end-effector's coordinate.

The divergence between $\boldsymbol{R_{iz}}$ and $\boldsymbol{s_n}$ can be represented by a rotation around an axis, $\boldsymbol{f_r}$, with angle θ_r.

$$\boldsymbol{f_r} = \boldsymbol{R_{iz}} \times \boldsymbol{s_n} \tag{39}$$

$$\theta_r = \cos^{-1}(\boldsymbol{R_{iz}} \bullet \boldsymbol{s_n}) \tag{40}$$

Apparently, $\boldsymbol{f_r}$ is on the x-y plane referring to the end-effector's coordinate. The proportional control law can be written as

$$\boldsymbol{R_d}(j) = \boldsymbol{R_i}(j)\Delta\boldsymbol{O}(j) \tag{41}$$

$$\Delta\boldsymbol{O}(j) = < \boldsymbol{f_r}, k_p\theta_r > \tag{42}$$

$\boldsymbol{R_d}(j)$ is the demand orientation at time $t = jT$ and $\Delta\boldsymbol{O}(j)$ is the orientation adjustment. k_p is the proportional gain. $< \boldsymbol{f_r}, k_p\theta_r >$ represents the rotation matrix around axis, $\boldsymbol{f_r}$, with angle $k_p\theta_r$. The combination of demand position $\boldsymbol{x_d}$, and orientation matrix $\boldsymbol{R_d}$ becomes the final demand posture, $\boldsymbol{X_d}$. Fig. 4 demonstrates the final block diagram with prediction of surface shape profile and normal direction, and orientation adjustment.

V. Validation Experiments and Discussion

The proposed force controller is applied on a 7DOF collaborative robot in order to test its validity and adaptiveness, as is shown in Fig. 1. A Maxwell 3-dimensional force sensor mounted on the end-effector provides measurement of external force for reference only.

Experiments include tracking along an inclined plane and a curved surface with constant normal contact force, which are simulations of polishing. Shape profiles of surfaces are treated as unknown in experiments. The contact force is estimated from joints' current information without any involvement of force sensor.

Favourable control parameters are listed in Table 1.

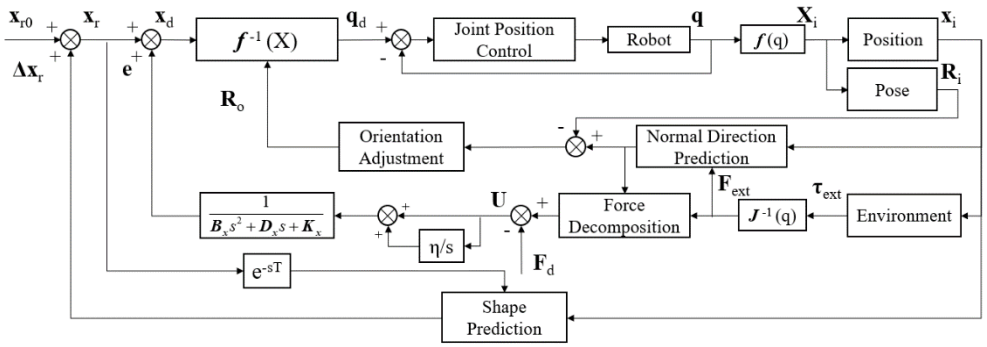

Fig. 4 Hybrid force controller with orientation adjustment and surface prediction.

Fig. 5 and Fig. 6 demonstrate the experiment process from (a) to (f). The robot started at the initial position and orientation. Then it moved along the surface with its orientation adjusting. After reaching the destination, the robot moved backward to the initial position.

Fig. 7 and Fig. 8 compare the measured and estimated contact force. In the upper part of each figure, the blue line stands for the contact force measured by the sensor while the red line for the estimated contact force along the predicted normal direction. In the lower part, the blue line stands for the difference between these two values while the red line for the deviation between the estimated force and desired force. The measured contact force along normal direction is replaced by its z-axis component relative to the end-effector coordinate. So, the difference between estimated force and measured force became larger when the robot is adjusting its orientation.

The root mean square error of force estimation for inclined surface tracking is 4.280N, and for curved surface tracking is 6.635N. It proves the credibility of sensorless force estimation.

The root mean square error of force controller for inclined surface tracking is 3.533N, and for curved surface tracking is 5.476N. The control accuracy is adequate for targeted applications and quite remarkable for sensorless force control [21-22]. Prediction algorithms, including the prediction of surface shape profile and normal direction, are also functional. These results indicate that under the given control parameters, the proposed force controller is effective and has preferable utility to arbitrary unknown surfaces.

VI. Conclusion

Manufacture methods for surface quality improvement have demanding requirements for the contact force exerted on the surface, especially the force along its normal direction. Thus, collaborative robot arms are more adequate for these applications than human workers. In this paper, an improved sensorless hybrid controller for constant normal force control is proposed for applications including polishing, milling and deburring.

Force control without any additional sensors is of great academic and practical value considering the hostile working environment and high hardware cost. An estimation method of external force/torque at end-effector, using joint current information, is applied on a 7DOF collaborative robot by considering joint friction model and dynamically consistent generalized inverse matrix. This method is also universal to industrial robots.

TABLE I
PARAMETERS FOR HYBRID FORCE CONTROLLER

Parameter	Value
Sampling Period	4ms
Stiffness of impedance model	1000N/m
Damping	20kg/s
Inertia	1kg
Integral coefficient	0.13
Desired contact force	50N
Velocity of the end-effector	5mm/s
Proportional gain for orientation adjustment	0.01

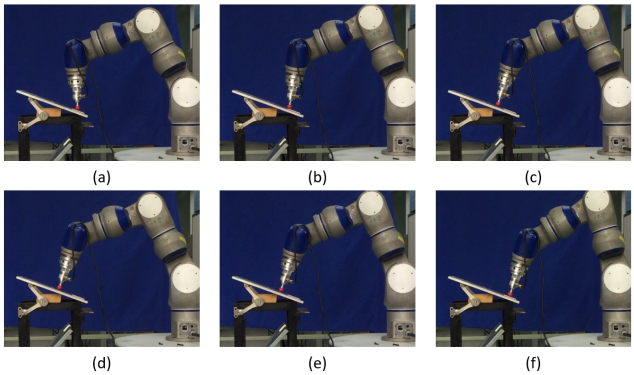

Fig. 5 The tracking process over an inclined plane

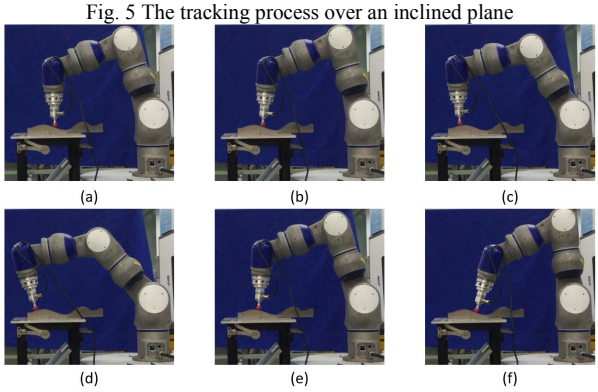

Fig. 6 The tracking process over a curved surface

The proposed force controller is based on the integration of impedance control and explicit force control. Position-based impedance control is adopted for its dependability. It realizes active compliance behaviour in Cartesian space. The idea of force deviation integral from explicit force control helps eliminate the steady state force error and improve tracking accuracy.

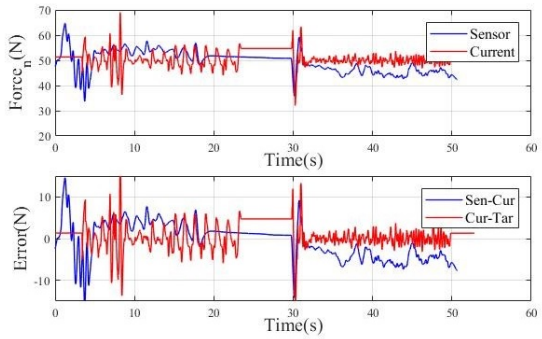

Fig. 7 Normal-force control result for plane tracking

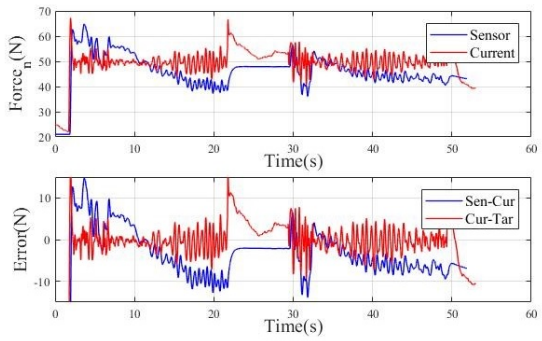

Fig. 8 Normal-force control result for curved surface tracking

The geometric information of the surface is a necessity. Instead of prior acquisition with high cost and time-consumption, a real-time algorithm for surface shape profile and normal direction prediction is proposed. The surface shape profile can be predicted from historical position information of end-effector, while the calculation of normal direction involves force information. This novel improvement enhances the adaptiveness and utility of the proposed force controller. Robot can adjust its end-effector's orientation to achieve better tracking accuracy and machine quality.

Experiments were performed to validate the proposed force controller, including tracking along an inclined plane and a curved surface. The results indicate that the external force estimation is credible. The accuracy of constant normal contact force control is adequate for targeted applications. The prediction algorithm is also effective in both situations as the robot adjusted its orientation according to the surface. It suggests that the proposed sensorless hybrid normal force controller can achieve preferable force control performance and good utility with arbitrary unknown surfaces.

The result indicates that the proposed force controller has certain merits and can replace force\torque sensors in applications where the accuracy meets the demand. Yet, there's still room for further research. In some special cases, not only the surface's geometric information, but also its dynamic characteristic needs prediction for greater adaptiveness.

REFERENCES

[1] L. Gracia, J. E. Solanes, P. Muñoz-Benavent, J. V. Miro, C. Perez-Vidal, and J. Tornero, "A Sliding Mode Control Architecture for Human-Manipulator Cooperative Surface Treatment Tasks," in *2018 IROS*, pp. 1318-1325.

[2] G. Xiong, Y. Ding and L. Zhu, "Stiffness-based pose optimization of an industrial robot for five-axis milling," *Robotics and Computer-Integrated Manufacturing,* vol. 55, pp. 19-28, 2019.

[3] A. E. K. Mohammad, J. Hong, D. Wang, and Y. Guan, "Synergistic integrated design of an electrochemical mechanical polishing end-effector for robotic polishing applications," *Robotics and Computer-Integrated Manufacturing,* vol. 55, pp. 65-75, 2019.

[4] C. Chen, F. Peng, R. Yan, Y. Li, D. Wei, Z. Fan, X. Tang, and Z. Zhu, "Stiffness performance index based posture and feed orientation optimization in robotic milling process," *Robotics and Computer-Integrated Manufacturing,* vol. 55, pp. 29-40, 2019.

[5] L. Villani and J. D. Schutter, "Force Control," in *Springer Handbook of Robotics*, 2016, pp. 161-185.

[6] H. Cho, M. Kim, H. Lim, and D. Kim, "Cartesian Sensor-less Force Control for Industrial Robots," in *2014 IROS*, pp. 4497-4502.

[7] A. Stolt, M. Linderoth, A. Robertsson, and R. Johansson, "Force Controlled Robotic Assembly without a Force Sensor," in *2012 ICRA*, pp. 1538-1543.

[8] L. Gao, J. Yuan, Z. Han, S. Wang, and N. Wang, "A Friction Model with Velocity, Temperature and Load Torque Effects for Collaborative Industrial Robot Joints," in *2017 IROS*, pp. 3027-3032.

[9] A. Wahrburg, J. Boes, K. D. Listmann, F. Dai, B. Matthias, and H. Ding, "Motor-Current-Based Estimation of Cartesian Contact Forces and Torques for Robotic Manipulators and Its Application to Force Control," *IEEE Transactions on Automation Science and Engineering,* vol. 15, pp. 879-886, 2018.

[10] C. Ott, A. Albu-Schaeffer, A. Kugi, and G. Hirzinger, "On the passivity-based impedance control of flexible joint robots," *IEEE Transactions on Robotics,* vol. 24, pp. 416-429, 2008.

[11] L. Roveda, F. Vicentini and L. M. Tosatti, "Deformation-tracking Impedance Control in interaction with Uncertain Environments," in *2013 IROS*, pp. 1992-1997.

[12] L. Gracia, J. Ernesto Solanes, P. Munoz-Benavent, J. V. Miro, C. Perez-Vidal, and J. Tornero, "Adaptive Sliding Mode Control for Robotic Surface Treatment Using Force Feedback," *Mechatronics,* vol. 52, pp. 102-118, 2018.

[13] G. Pugach, A. Melnyk, O. Tolochko, A. Pitti, and P. Gaussier, "Touch-based Admittance Control of a Robotic Arm using Neural Learning of an Artificial Skin," in *2016 IROS*, 2016, pp. 3374-3380.

[14] F. Chen, H. Zhao, D. Li, L. Chen, C. Tan, and H. Ding, "Contact force control and vibration suppression in robotic polishing with a smart end effector," *Robotics and Computer-Integrated Manufacturing,* vol. 57, pp. 391 - 403, 2019.

[15] C. Schindlbeck and S. Haddadin, "Unified Passivity-Based Cartesian Force/Impedance Control for Rigid and Flexible Joint Robots via Task-Energy Tanks," in *2015 ICRA*, pp. 440-447.

[16] E. Shahriari, A. Kramberger, A. Gams, A. Ude, and S. Haddadin, "Adapting to Contacts: Energy Tanks and Task Energy for Passivity-Based Dynamic Movement Primitives," in *IEEE-RAS International Conference on Humanoid Robotics*, 2017, pp. 136-142.

[17] J. Yuan, Y. Qian, Z. Yuan, L. Gao and W. Wan, " Position based Impedance Force Control ler with Sensorless Force Estimation," in *Assembly Automation*, 2019,vol. 39 No. 3 pp 489-496.

[18] S. Jung, "A position-based force control approach to a quad-rotor system," in *Ubiquitous Robots and Ambient Intelligence,* 2012, pp. 373-377.

[19] K. Lee and M. Buss, "Force tracking impedance control with variable target stiffness," *IFAC Proceedings Volumes,* vol. 41, pp. 6751-6756, 2008.

[20] A. Gams, T. Petric, M. Do, B. Nemec, J. Morimoto, T. Asfour, and A. Ude, "Adaptation and coaching of periodic motion primitives through physical and visual interaction," *Robotics and Autonomous Systems,* vol. 75, pp. 340-351, 2016.

[21] I. Tyapin, K. B. Kaldestad and G. Hovland, "Off-line Path Correction of Robotic Face Milling Using Static Tool Force and Robot Stiffness.," in *2015 IROS*, pp. 5506-5511.

[22] L. Cen and S. N. Melkote, "Effect of Robot Dynamics on the Machining Forces in Robotic Milling," in *Procedia Manufacturing*, 2017, pp. 486-496.